

OPTICS

Efficient light-emitting diodes based on oriented perovskite nanoplatelets

Jieyuan Cui^{1†}, Yang Liu^{2†}, Yunzhou Deng^{1†}, Chen Lin^{3†}, Zhishan Fang³, Chensheng Xiang⁴, Peng Bai⁵, Kai Du⁴, Xiaobing Zuo⁶, Kaichuan Wen⁷, Shaolong Gong⁸, Haiping He³, Zhizhen Ye^{3,9*}, Yunan Gao⁵, He Tian⁴, Baodan Zhao¹⁰, Jianpu Wang⁷, Yizheng Jin^{1*}

Solution-processed planar perovskite light-emitting diodes (LEDs) promise high-performance and cost-effective electroluminescent devices ideal for large-area display and lighting applications. Exploiting emission layers with high ratios of horizontal transition dipole moments (TDMs) is expected to boost the photon outcoupling of planar LEDs. However, LEDs based on anisotropic perovskite nanoemitters remain to be inefficient (external quantum efficiency, EQE <5%) due to the difficulties of simultaneously controlling the orientations of TDMs, achieving high photoluminescence quantum yields (PLQYs) and realizing charge balance in the films of assembled nanostructures. Here, we demonstrate efficient electroluminescence from an in situ grown perovskite film composed of a monolayer of face-on oriented nanoplatelets. The ratio of horizontal TDMs of the perovskite nanoplatelet film is ~84%, which leads to a light-outcoupling efficiency of ~31%, substantially higher than that of isotropic emitters (~23%). In consequence, LEDs with a peak EQE of 23.6% are achieved, representing highly efficient planar perovskite LEDs.

INTRODUCTION

Photon emission characteristics in semiconductors are mediated by transition dipole moments (TDMs). The optical TDMs of inorganic nanostructures with reduced dimensions, such as nanoplatelets and nanorods, are highly anisotropic (1–4). This unique structure-property relationship is of interest for planar light-emitting diodes (LEDs) because the outcoupling efficiency of the devices is fundamentally correlated to the orientation of emissive TDMs (5–9). In general, TDMs that are horizontally oriented with respect to the electrode interface are favored for light outcoupling, while the vertically oriented TDMs largely contribute to the energy loss (see figs. S1 and S2 for detailed illustrations) (10).

Metal halide perovskite is an emerging class of solution-processed semiconductors with intriguing properties, such as high photoluminescence quantum yields (PLQYs) and tunable emission wavelengths (11–13). Since the first report of the room temperature-operating perovskite LEDs (PeLEDs) in 2014 (14), remarkable

progress has been made on device efficiency (15–26). We note that these state-of-the-art planar PeLEDs are based on films with isotropic TDMs (table S1). Enhancing the ratio of horizontally oriented TDMs is expected to further improve light outcoupling and boost the upper limit for the external quantum efficiencies (EQEs) of PeLEDs.

Here, we report efficient LEDs based on in situ grown perovskite films, which simultaneously demonstrate high ratios of horizontal TDMs and high PLQYs. The emitters are oriented perovskite nanoplatelets with a high in-plane TDM ratio of ~84%, leading to LEDs with a light extraction efficiency of ~31%. In contrast, using isotropic emitters (in-plane TDM ratio of 67%) in the same device structure would limit the light extraction efficiency to ~23%. Furthermore, we find that the PLQY of the perovskite film can be boosted to more than 75% by introducing lithium bromide (LiBr) into the precursor solution. These combined efforts enable green PeLEDs with a record EQE of 23.6%, the highest value in planar PeLEDs.

RESULTS

Structural characterization of the in situ formed nanoplatelets

Figure 1A shows a cross-sectional view of our device, including the perovskite layer, analyzed by aberration-corrected scanning transmission electron microscopy (STEM). Our devices consist of multilayers of nickel oxide (NiO; ~7 nm), poly(9,9-dioctylfluorene-co-N-(4-butylphenyl)-diphenylamine)/poly(9-vinylcarbazole) (TFB/PVK, ~38 nm), perovskite (~9 nm), 2,2',2''-(1,3,5-benzotriptyl) tris(1-phenyl-1H-benzimidazole) (TPBi; ~48 nm), lithium fluoride (LiF; ~1 nm), and aluminum (Al; ~100 nm) sequentially deposited onto indium tin oxide (ITO)-coated glass substrates (see Materials and Methods for details). The perovskite film was deposited from a precursor solution comprising LiBr, phenylbutylammonium bromide (PBABr), phenylethyl-ammonium bromide (PEABr), cesium bromide (CsBr), and lead bromide (PbBr₂) dissolved in dimethyl sulfoxide (DMSO) with a molar ratio of 0.25:0.75:0.25:1.75:1.4.

¹Zhejiang Key Laboratory for Excited-State Materials, State Key Laboratory of Silicon Materials, Department of Chemistry, Zhejiang University, Hangzhou 310027, China.

²Zhejiang Key Laboratory for Excited-State Materials, State Key Laboratory of Silicon Materials, School of Materials Science and Engineering, Zhejiang University, Hangzhou 310027, China. ³State Key Laboratory of Silicon Materials, School of Materials Science and Engineering, Zhejiang University, Hangzhou 310027, China.

⁴Centre of Electron Microscope, State Key Laboratory of Silicon Materials, School of Materials Science and Engineering, Zhejiang University, Hangzhou 310027, China.

⁵China State Key Laboratory for Artificial Microstructure and Mesoscopic Physics, School of Physics, Peking University, Beijing 100871, China. ⁶X-Ray Science Division, Argonne National Laboratory, 9700 South Cass Avenue, Argonne, IL 60439, USA.

⁷Key Laboratory of Flexible Electronics (KLOFE), Institute of Advanced Materials (IAM), Jiangsu National Synergetic Innovation Centre for Advanced Materials (SICAM), Nanjing Tech University (NanjingTech), 30 South Puzhu Road, Nanjing 211816, China. ⁸Department of Chemistry, Hubei Key Lab on Organic and Polymeric Optoelectronic Materials, Wuhan University, Wuhan 430072, China. ⁹ZJU-WZ Novel Materials Science & Technology Innovation Center, Institute of Wenzhou, Zhejiang University, Wenzhou 325006, China. ¹⁰State Key Laboratory of Modern Optical Instrumentation, College of Optical Science and Engineering, International Research Center for Advanced Photonics, Zhejiang University, Hangzhou 310027, China.

*Corresponding author. Email: yezz@zju.edu.cn (Z.Y.); yizhengjin@zju.edu.cn (Y.J.)

†These authors contributed equally to this work.

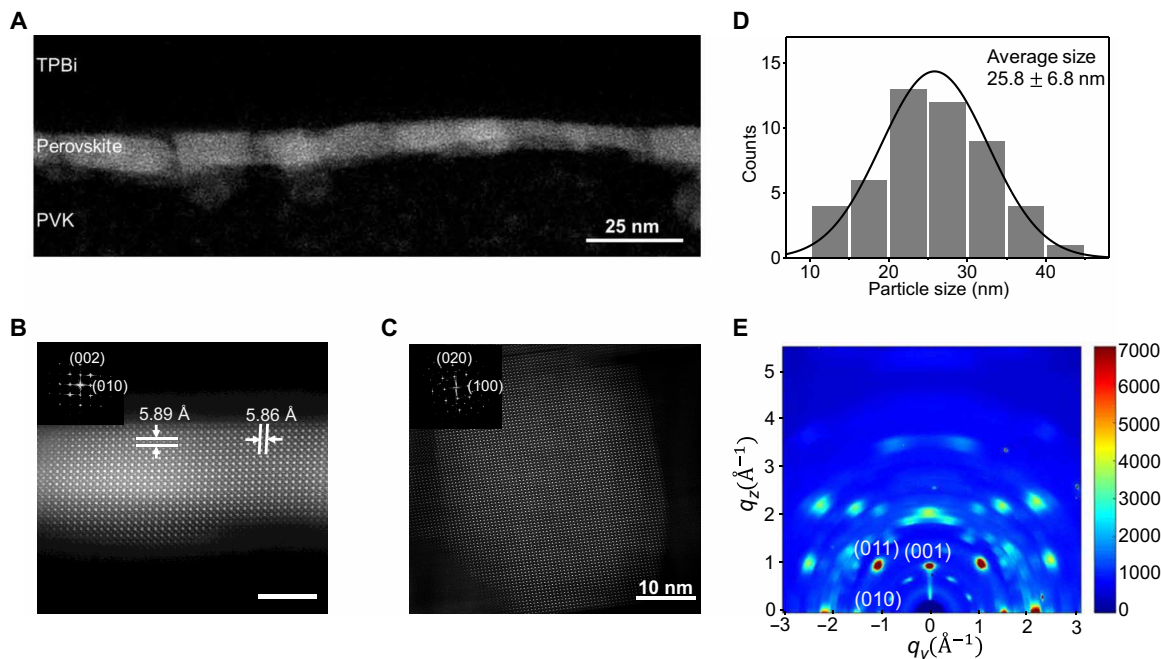


Fig. 1. Structural characterizations of the perovskite nanoplatelet films. (A) A cross-sectional scanning transmission electron microscopy–high-angle annular dark-field (STEM-HAADF) image showing the continuous and pinhole-free perovskite layer. TPBi, 2,2',2''-(1,3,5-benzinetriyl)tris(1-phenyl-1*H*-benzimidazole); PVK, poly(9-vinylcarbazole). (B) A zoomed-in STEM-HAADF image showing the fine structure of a perovskite nanoplatelet. Inset: The corresponding fast Fourier transform (FFT) pattern. (C) A typical high-resolution transmission electron microscopy (HRTEM) image of the perovskite nanoplatelets dispersed on a copper grid. Inset: The corresponding FFT pattern. (D) Statistical diagram of the size distribution of the nanoplatelets measured by HRTEM. The average size is 25.8 nm and the corresponding SD is 6.8 nm. The Gaussian fitting is provided as a guide to the eye. (E) Grazing-incidence wide-angle x-ray scattering pattern. The diffraction spots originate from the crystal faces of nanoplatelets. The two diffraction spots at $q_z = 1.065$ and $q_y = 1.070 \text{ \AA}^{-1}$ correspond to {001} and {010} of β -CsPbBr₃, respectively.

The high-angle annular dark-field (HAADF) image indicates a continuous and pinhole-free perovskite film with a thickness of $8.6 \pm 1.5 \text{ nm}$ (Fig. 1A and fig. S3). Zoom-in observations (Fig. 1B) show an atomic-resolution image with well-resolved atom columns, revealing the high crystallinity of the perovskite nanoplatelets. The crystal structure of the nanoplatelet matches that of tetragonal β -CsPbBr₃ (27). The perovskite crystal is oriented with the {001} crystal face parallel to the substrate surface. Atomic force microscopy characterizations on a perovskite film show a low root mean square surface roughness of $\sim 1.2 \text{ nm}$ (fig. S4), which is in line with the cross-sectional observations. The perovskite nanoplatelets were transferred and dispersed onto a copper grid for high-resolution transmission electron microscopy (HRTEM) analyses (28). The results (Fig. 1C and fig. S5) indicate that the perovskite crystals are nanoplatelets with an average lateral size of $25.8 \pm 6.8 \text{ nm}$ (Fig. 1D). The Grazing-incidence wide-angle x-ray scattering (GIWAXS) measurement (Fig. 1E) of a perovskite film shows discrete diffraction spots. The diffraction spot on $q_z = 1.065 \text{ \AA}^{-1}$ corresponds to a real-space distance of 5.89 \AA , which can be assigned as the d -spacing of the {001} crystal face of tetragonal β -CsPbBr₃. These features suggest that the assemblies of the perovskite nanoplatelets are highly ordered and all nanoplatelets share the same orientation with the {001} crystal face parallel to the substrate. The GIWAXS data, together with the STEM-HAADF and HRTEM observations, suggest that the perovskite films consist of a monolayer of face-on oriented nanoplatelets with an average thickness of $8.6 \pm 1.5 \text{ nm}$ and a lateral size of $25.8 \pm 6.8 \text{ nm}$.

Optical analyses of the in situ formed nanoplatelet film

We expect the electronic and optical properties of the perovskite film to be influenced by the quantum confinement effect because the out-of-plane dimension of the nanoplatelets is comparable to the Bohr diameter of CsPbBr₃ (7 nm) (29). The photoluminescence (PL) spectrum of the perovskite film shows the symmetric shape and its peak position is at 516 nm (Fig. 2A), corresponding to an optical bandgap of 2.41 eV. This value is larger than the bandgap of bulk β -CsPbBr₃, $\sim 2.36 \text{ eV}$ (30). The excitonic absorption features of quasi-two-dimensional (2D) perovskites in the strong confinement regime, such as $n = 2$ and $n = 3$ (n is the number of PbBr₄ octahedral layers within a crystallite) layered perovskites, are absent in the ultraviolet-visible absorption spectrum (Fig. 2A). This feature suggests that our film composed of perovskite nanoplatelets is distinctive from the previously reported perovskite films of multiple quantum wells or quantum dots embedded in quasi-2D phase (16, 17, 22). The perovskite nanoplatelet film exhibits a high PLQY of $\sim 75\%$ at a low excitation power density of $\sim 0.02 \text{ mW/cm}^2$ (Fig. 2B). This result indicates efficient radiative recombination of the photogenerated excitons in the perovskite nanoplatelets.

The orientation of TDMs of the perovskite nanoplatelet film is quantified by the ratio of horizontal TDMs, Θ . This parameter is defined as $\Theta = p_{\parallel} / (p_{\parallel} + p_{\perp})$, where p_{\parallel} and p_{\perp} stand for contributions from horizontal and vertical components of the optical TDMs, respectively. We used the angle-dependent PL technique, which provides an ensemble measurement (photoexcitation spot size: $\sim 1 \text{ mm}$) of the intensity of p-polarized emission against the detection angle

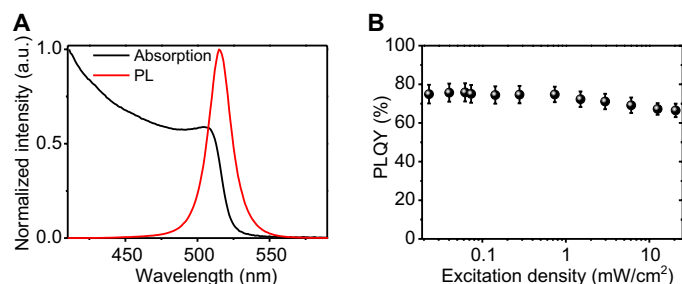


Fig. 2. Optical properties of the perovskite nanoplatelet films. (A) Absorption and PL (excited by a 405-nm laser) spectra, a.u., arbitrary units. (B) Excitation intensity-dependent PLQY. The error bars represent the experimental uncertainties in the PLQY measurements at 0.4 mW/cm² and the errors in the determination of relative PL intensities and excitation power.

(see fig. S6 for schematic illustration) (7, 31, 32). The experimental data (Fig. 3A) are fitted to the pattern simulated using the classical dipole radiation model (10, 33, 34). The Θ of our perovskite nanoplatelet film is determined to be 84%. This value is substantially higher than that of isotropic emitters (67%). Furthermore, we analyzed the light emission of the perovskite film by using back focal plane (BFP) spectroscopy. BFP spectroscopy (see fig. S7 for schematic illustration) probes a small targeted region of the perovskite nanoplatelet film by using a laser with a spot size of ~ 750 nm for photoexcitation (1–3, 35). The BFP pattern and the corresponding line-cut data along the p-polarized direction are shown in Fig. 3 (B and C, respectively). An important feature of the horizontally oriented dipoles is that the p-polarized intensity is minimum at $k_{\parallel} = k_0$, where k_{\parallel} is the in-plane wave vector with respect to the substrate and k_0 is the wave vector in the vacuum. By fitting the line-cut data in Fig. 3C, Θ is determined to be $\sim 87\%$. The BFP data of four spots from different regions (fig. S8) demonstrate excellent spatial uniformity of the orientations of TDMs in our film. The results of both measurements unambiguously demonstrate that the emission of our perovskite nanoplatelet film is dominated by horizontal TDMs.

We suggest that the anisotropy of local fields in the nanoplatelet, i.e., dielectric confinement, largely contributes to the anisotropy of the dipole orientation (3, 36). The local electric field normal to the nanoplatelet plane, E_{\perp} , is reduced (screened) due to the dielectric confinement, while the local field in the horizontal directions, E_{\parallel} , is less affected. The spontaneous radiative transition probability of the nanoplatelet, which is proportional to the square of local fields, is thus substantially reduced in the normal direction. For our closely packed oriented nanoplatelets, the local field in the horizontal directions is expected to be even less affected owing to the near continuum of the high dielectric constant perovskite material in the lateral directions.

Key factors affecting the perovskite films

Two issues, namely, the concentrations of the bulky organic ammonium cations and the introduction of LiBr in the precursor solution, are critical for the formation of oriented perovskite nanoplatelet film with high PLQY. Without the use of the bulky organic ammonium cations, the resulting perovskite film shows an optical bandgap of ~ 2.37 eV (fig. S9A) and excitation intensity-dependent PLQY (fig. S9C). These features indicate the formation of 3D CsPbBr₃ crystals. Doubling the concentration of the bulky organic ammonium cations leads to the formation of perovskite films with

strong excitonic absorption peaks at ~ 430 , ~ 460 , and ~ 475 nm, which corresponds to the $n = 2$, $n = 3$, and $n = 4$ layered perovskites, respectively (fig. S9B). The emission peak of this perovskite film locates at ~ 501 nm, implying efficient energy transfer from the perovskites with small n values (larger bandgaps) to the emissive centers with smaller bandgaps. The emissive centers are determined to be nanocrystals with a size of ~ 10 nm (fig. S9D). BFP measurements on the films processed from the precursor solution with various contents of bulky organic ammonium cations indicate that only the oriented perovskite nanoplatelet films have high ratios of horizontal TDMs (fig. S10). Furthermore, control experiments show that other investigated parameters, i.e., the concentration of the precursor solution, the choice of bulky organic ligands, and the underlying substrates, have little impacts on the Θ values of perovskite films (fig. S11). We suggest that the horizontal orientation of the perovskite nanoplatelets on flat substrates may originate from the van der Waals interactions as reported in the literature (37, 38). Besides, the ultrathin film of ~ 9 nm would also favor horizontally aligned perovskite nanoplatelets (39).

Further experiments show that the introduction of LiBr in the precursor solution is beneficial for improving the PLQY of the perovskite film. GIWAXS, angle-dependent PL, and BFP measurements (fig. S12) on the perovskite films processed from the precursor solution without LiBr indicate the formation of oriented nanoplatelets with anisotropic emission (Θ : 84%). The PLQY of perovskite nanoplatelet films processed from the precursor solution with and without LiBr is $\sim 75\%$ and $\sim 50\%$ (fig. S13), respectively. Temperature-dependent PL characterizations (fig. S14) indicate a scenario that the with-Li sample has fewer energy levels below excitonic levels and, thereby, fewer nonradiative losses of photo-generated excitons. We suggest that the introduction of LiBr in the precursor solution may result in perovskite nanoplatelets with better surface passivation.

Characterization of the PeLEDs

The electroluminescence (EL) spectrum of our perovskite nanoplatelet film (Fig. 4A) displays a symmetric peak centered at ~ 518 nm with a full width at half maximum of 16 nm (74 meV), representing one of the narrowest emission line widths for high-efficiency PeLEDs (20, 24–26, 40–42). The ultrapure green emission corresponds to Commission Internationale de l'Éclairage color coordinates of (0.09, 0.78) (fig. S15). The angular emission intensity of our PeLEDs follows the Lambertian profile (Fig. 4B). The EL spectra at different viewing angles are identical (fig. S16). The current density–voltage–luminance curves of a typical device are shown in Fig. 4C. Owing to the pinhole-free morphology of the nanoplatelet film, the device shows negligible leakage current. The current density and luminance increase rapidly once a turn-on voltage of ~ 3 V is reached. At 7 V, the device shows a brightness of ~ 3140 cd/m². The champion device demonstrates a peak EQE of 23.6% (Fig. 4D), which is a record efficiency among PeLEDs (table S1). The statistical diagram of 36 devices (Fig. 4E) indicates an average EQE of 21.3% with a small relative SD of 4.4% demonstrating the excellent reproducibility of our green LEDs. The device shows a typical T_{50} lifetime of ~ 15 min at an initial luminance of ~ 1080 cd/m² (fig. S17).

We performed optical simulations on the PeLEDs by using the classical dipole model developed for planar microcavities (see fig. S18 for details) (33, 34). The result suggests a light-outcoupling efficiency of 31.1% for our perovskite devices based on the oriented nanoplatelet film with Θ of 84% (fig. S18B). In contrast, a control

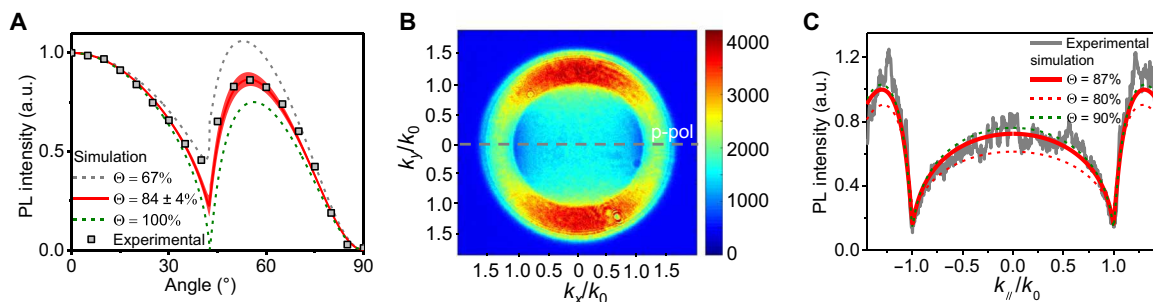


Fig. 3. Orientations of the TDMs of the perovskite nanoplatelet films. (A) Angle-dependent PL measurements of the perovskite film on a quartz/TFB/PVK substrate. The experimental data (gray squares) are fitted by the classical electromagnetic dipole model (red line), giving a horizontal TDM ratio of $84 \pm 4\%$. (B) Back focal plane (BFP) image of a perovskite film. (C) p-polarized line cut (gray line) along the dashed line in of the BFP image (B). This line cut is fitted with a horizontal TDM ratio of 87% (red solid line).

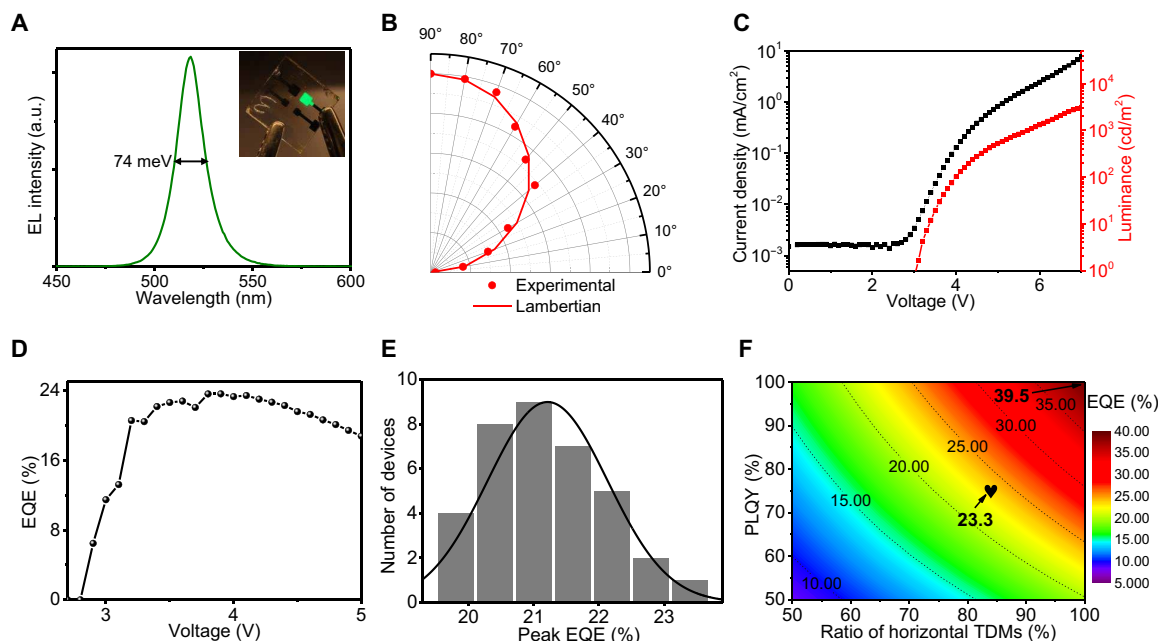


Fig. 4. Device characterizations of the green LEDs based on the perovskite nanoplatelet films. (A) EL spectrum. Inset: Photograph of an operating green LED (effective area: 3.24 mm^2). (B) Angular distribution of the EL intensity follows the Lambertian profile. (C) Current density–luminance–voltage characteristics of a typical device. (D) EQE–voltage relationship of the device with a champion EQE of 23.6%. (E) Histogram of peak EQEs from 36 devices. The Gaussian fits are provided as a guide to the eye. (F) Contour plot of the simulation results of device EQE as a function of PLQY and Θ of the perovskite emissive layer. The device structure shown in (A) is used for the simulation. The refractive indexes of the multilayers are obtained by ellipsometer. For our perovskite nanoplatelet film with a PLQY of $\sim 75\%$ and a Θ of 84%, the optical simulation predicts a maximum EQE of $\sim 23.3\%$.

device based on isotropic TDMs (Θ : 67%) would have a lower outcoupling efficiency of $\sim 23.4\%$. Considering that the PLQY of our perovskite nanoplatelet film is $\sim 75\%$, our optical simulation predicts a maximum EQE of 23.3% (Fig. 4F), which agrees well with the experimental results. Further optimizing the PLQY and enhancing Θ of the perovskite films shall push the upper limit of EQEs to $\sim 40\%$ (Fig. 4F).

We highlight that previous work aiming to control the orientations of TDMs focuses on assemblies of anisotropic colloidal nanostructures (43–46). High-efficiency EL would require syntheses of anisotropic colloidal nanostructures with high PLQY controlling the orientations of the anisotropic colloidal nanostructures to realize films with high ratios of horizontal TDMs, minimizing energy transfer between the neighboring nanoemitters to maintain high PLQYs and efficient and balanced charge injection into the individual

nanoemitters. Fulfilling these stringent requirements is challenging and often imposes dilemmas in material design and assembly. As a result, the EQEs of the LEDs based on colloidal anisotropic perovskite nanoemitters are currently lower than 5% (see table S2 for more information) (47). Expanding the scope to all solution-processed planar LEDs using inorganic emitters with oriented TDMs (table S2), the reported highest EQE is 12.1% (43). In contrast, our LEDs based on in situ grown perovskite nanoplatelet films demonstrate high EQEs of up to 23.6%.

DISCUSSION

We demonstrate that controlling the orientation of TDMs of the perovskite films overcomes the light-outcoupling limitation of

planar LEDs with isotropic emitters, leading to green LEDs with exceptionally high EQEs of up to 23.6%. Considering the chemical versatility of perovskite materials, our facile approach of in situ grown nanoplatelet films is readily extended to the fabrication of differently colored LEDs with high EQEs. Our work represents a simple yet effective approach of exploiting anisotropic optical properties of nanostructures in optoelectronic devices.

MATERIALS AND METHODS

Materials

TFB was purchased from American Dye Source. PBA (>98.0%), PEA (>98.0%), nickel acetate tetrahydrate (>99.0%), and chlorobenzene (99.8%) were purchased from Acros. DMSO (99.9%), CsBr (99.999%), LiF (99.99%), and hydrobromic acid (48 weight % in water) were purchased from Alfa Aesar. PVK (with a molecular weight of 25,000 to 50,000 g mol⁻¹), LiBr (99.999%), ethanolamine (99%), and PbBr₂ (99.999%) were purchased from Sigma-Aldrich. TPBi was purchased from Xi'an Polymer Light Technology Corp.

NiO_x precursor was prepared by following a literature method (48). PBABr and PEABr were synthesized following the instruction of the previous report (28). Briefly, hydrobromic acid (2.56 ml) was slowly added into a solution of PEA (3 ml) in methanol (20 ml) at 0°C, and then stirred for 2 hours. Next, the solution was evaporated at 45°C to obtain precipitates, which were washed thrice with a mixed solution of ethyl acetate and diethyl ether with a volume ratio of 1:1. Then, the precipitates were dried at 50°C in the vacuum for 24 hours.

The precursor solution for the perovskite nanoplatelet film was prepared by mixing a CsPbBr₃ precursor solution (1 ml), a LiBr precursor solution (0.25 ml), and DMSO (0.5 ml). The CsPbBr₃ precursor solution was prepared by mixing PBABr (18.9 mg), PEABr (5.5 mg), CsBr (40.8 mg), and PbBr₂ (56.2 mg) in DMSO (1 ml) followed by stirring for 2 hours at 50°C. The LiBr precursor solution was prepared by dissolving LiBr (9.55 mg) in DMSO (1 ml).

Device fabrication

The NiO_x precursor was deposited on ITO-coated glass substrates (square resistance of 20 ohms) by a literature method (22). The TFB (in chlorobenzene, 8 mg/ml) was spin-coated at 2000 rpm and then annealed at 150°C for 30 min. Then, the TFB film was spin-rinsed by chlorobenzene, leaving an ultrathin layer. Next, the PVK layer was deposited by spin-coating PVK solution (in chlorobenzene, 14 mg/ml) at 2000 rpm, followed by annealing at 150°C for 30 min. The perovskite film was prepared by spin-coating the precursor solution at 4000 rpm for 2 min, followed by annealing at 100°C for 25 min. Next, the TPBi (48 nm), LiF (1 nm), and Al (100 nm) were sequentially deposited by using a thermal evaporating system (Trovato C300) at a high-vacuum environment (under 2×10^{-7} torr). The device area defined by the overlapping area of the ITO and Al electrodes was 3.24 mm².

Structural and optical characterizations

The cross-sectional samples were prepared by using focused ion beam equipment (Quata 3D FEG). The TEM observations were conducted using a Cs aberration-corrected scanning transmission electron microscope, Titan G2 80-200 ChemiSTEM microscope, operated at 200 kV.

Atomic force microscopy analyses were conducted with a Cypher-S (Asylum Research) atomic force microscope located in a glovebox filled with nitrogen. GIWAXS measurements were performed at Beamline 12-ID-B of Advanced Photon Source (Argonne National Laboratory, USA). A PerkinElmer detector, XRpad 4343F, was applied in the measurements with a sample-to-detector distance of 18 cm. The energy of x-ray radiation was 13.3 keV.

The angle-dependent PL spectra of the perovskite nanoplatelet films (deposited on quartz/TFB/PVK substrate) were collected by using a molecular orientation characteristic measurement system C14234-11 (Hamamatsu Photonics K.K., Japan; fig. S6). The range of angles is 0° to 90°. The excitation wavelength is 365 nm.

The BFP imaging experiments were performed on an optical system as schematically shown in fig. S7. The excitation wavelength is 457 nm and the diameter of the excitation spot is ~750 nm.

The refractive index (*n*) and extinction coefficient (*k*) of all layers of the PeLEDs were measured by an ellipsometer (J.A. Woollam, USA). Ultraviolet-visible absorption spectra of the samples were collected by using a Cary 5000 (Agilent) spectrophotometer.

Steady-state PL, transient PL, and temperature-dependent PL spectra were performed on an Edinburgh Instruments (FLS920) spectrometer. Excitation density-dependent PLQYs of the perovskite films were obtained by following the published method (22). The angle dependence of emission intensity of the PeLED was measured using a Thorlabs PDA100A detector at a fixed distance of 200 mm from the EL device (16).

All LEDs were measured in a glovebox filled with nitrogen at room temperature. A system consisting of an integration sphere (FOIS-1), a Keithley 2400 source meter, and a QE-Pro spectrometer (Ocean Optics) was used for the measurements (49). The devices were scanned from zero bias at a rate of 0.1 V s⁻¹. The integral time for each step is 500 ms. The EL characteristics of the LEDs were cross-checked at Zhejiang University (Yizheng Jin group), University of Cambridge (Richard Friend group), and Nanjing Tech University (Jianpu Wang group).

SUPPLEMENTARY MATERIALS

Supplementary material for this article is available at <https://science.org/doi/10.1126/sciadv.abg8458>

REFERENCES AND NOTES

1. R. Scott, J. Heckmann, A. V. Prudnikau, A. Antanovich, A. Mikhailov, N. Owschmikov, M. Artemyev, J. I. Climente, U. Woggon, N. B. Grosse, A. W. Achtstein, Directed emission of CdSe nanoplatelets originating from strongly anisotropic 2D electronic structure. *Nat. Nanotechnol.* **12**, 1155–1160 (2017).
2. Y. Gao, M. C. Weidman, W. A. Tisdale, CdSe nanoplatelet films with controlled orientation of their transition dipole moment. *Nano Lett.* **17**, 3837–3843 (2017).
3. M. J. Jurow, T. Morgenstern, C. Eisler, J. Kang, E. Penzo, M. Do, M. Engelmayr, W. T. Osowiecki, Y. Bekenstein, C. Tassone, L. W. Wang, A. P. Alivisatos, W. Brütting, Y. Liu, Manipulating the transition dipole moment of CsPbBr₃ perovskite nanocrystals for superior optical properties. *Nano Lett.* **19**, 2489–2496 (2019).
4. J. Jagielski, S. F. Solari, L. Jordan, D. Scullion, B. Blulle, Y. T. Li, F. Krumeich, Y. C. Chiu, B. Ruhstaller, E. J. G. Santos, C. J. Shih, Scalable photonic sources using two-dimensional lead halide perovskite superlattices. *Nat. Commun.* **11**, 387 (2020).
5. J.-S. Kim, P. K. H. Ho, N. C. Greenham, R. H. Friend, Electroluminescence emission pattern of organic light-emitting diodes: Implications for device efficiency calculations. *J. Appl. Phys.* **88**, 1073–1081 (2000).
6. X.-W. Chen, W. C. H. Choy, S. He, Efficient and rigorous modeling of light emission in planar multilayer organic light-emitting diodes. *J. Disp. Technol.* **3**, 110–117 (2007).
7. S.-Y. Kim, W.-I. Jeong, C. Mayr, Y.-S. Park, K.-H. Kim, J.-H. Lee, C.-K. Moon, W. Brütting, J.-J. Kim, Organic light-emitting diodes with 30% external quantum efficiency based on a horizontally oriented emitter. *Adv. Funct. Mater.* **23**, 3896–3900 (2013).

8. T.-L. Wu, M.-J. Huang, C.-C. Lin, P.-Y. Huang, T.-Y. Chou, R.-W. Chen-Cheng, H.-W. Lin, R.-S. Liu, C.-H. Cheng, Diboron compound-based organic light-emitting diodes with high efficiency and reduced efficiency roll-off. *Nat. Photonics* **12**, 235–240 (2018).
9. G. Walters, L. Haeberle, R. Quintero-Bermudez, J. Brodeur, S. Kena-Cohen, E. H. Sargent, Directional light emission from layered metal halide perovskite crystals. *J. Phys. Chem. Lett.* **11**, 3458–3465 (2020).
10. W. L. Barnes, Fluorescence near interfaces: The role of photonic mode density. *J. Mod. Opt.* **45**, 661–699 (1998).
11. B. R. Sutherland, E. H. Sargent, Perovskite photonic sources. *Nat. Photonics* **10**, 295–302 (2016).
12. S. D. Stranks, H. J. Snaith, Metal-halide perovskites for photovoltaic and light-emitting devices. *Nat. Nanotechnol.* **10**, 391–402 (2015).
13. X. K. Liu, W. Xu, S. Bai, Y. Jin, J. Wang, R. H. Friend, F. Gao, Metal halide perovskites for light-emitting diodes. *Nat. Mater.* **20**, 10–21 (2021).
14. Z. K. Tan, R. S. Moghaddam, M. L. Lai, P. Docampo, R. Higler, F. Deschler, M. Price, A. Sadhanala, L. M. Pazos, D. Credgington, F. Hanusch, T. Bein, H. J. Snaith, R. H. Friend, Bright light-emitting diodes based on organometal halide perovskite. *Nat. Nanotechnol.* **9**, 687–692 (2014).
15. H. C. Cho, S. H. Jeong, M. H. Park, Y. H. Kim, C. Wolf, C. L. Lee, J. H. Heo, A. Sadhanala, N. Myoung, S. Yoo, S. H. Im, R. H. Friend, T. W. Lee, Overcoming the electroluminescence efficiency limitations of perovskite light-emitting diodes. *Science* **350**, 1222–1225 (2015).
16. N. Wang, L. Cheng, R. Ge, S. Zhang, Y. Miao, W. Zou, C. Yi, Y. Sun, Y. Cao, R. Yang, Y. Wei, Q. Guo, Y. Ke, M. Yu, Y. Jin, Y. Liu, Q. Ding, D. Di, L. Yang, G. Xing, H. Tian, C. Jin, F. Gao, R. H. Friend, J. Wang, W. Huang, Perovskite light-emitting diodes based on solution-processed self-organized multiple quantum wells. *Nat. Photonics* **10**, 699–704 (2016).
17. M. Yuan, L. N. Quan, R. Comin, G. Walters, R. Sabatini, O. Voznyy, S. Hoogland, Y. Zhao, E. M. Beauregard, P. Kanjanaboos, Z. Lu, D. H. Kim, E. H. Sargent, Perovskite energy funnels for efficient light-emitting diodes. *Nat. Nanotechnol.* **11**, 872–877 (2016).
18. Z. Xiao, R. A. Kerner, L. Zhao, N. L. Tran, K. M. Lee, T.-W. Koh, G. D. Scholes, B. P. Rand, Efficient perovskite light-emitting diodes featuring nanometre-sized crystallites. *Nat. Photonics* **11**, 108–115 (2017).
19. Y. Cao, N. Wang, H. Tian, J. Guo, Y. Wei, H. Chen, Y. Miao, W. Zou, K. Pan, Y. He, H. Cao, Y. Ke, M. Xu, Y. Wang, M. Yang, K. Du, Z. Fu, D. Kong, D. Dai, Y. Jin, G. Li, H. Li, Q. Peng, J. Wang, W. Huang, Perovskite light-emitting diodes based on spontaneously formed submicrometre-scale structures. *Nature* **562**, 249–253 (2018).
20. K. Lin, J. Xing, L. N. Quan, F. P. G. de Arquer, G. Gong, J. Lu, L. Xie, W. Zhao, D. Zhang, C. Yan, W. Li, X. Liu, Y. Lu, J. Kirman, E. H. Sargent, Q. Xiong, Z. Wei, Perovskite light-emitting diodes with external quantum efficiency exceeding 20 percent. *Nature* **562**, 245–248 (2018).
21. B. Zhao, S. Bai, V. Kim, R. Lamboll, R. Shivanna, F. Auras, J. M. Richter, L. Yang, L. Dai, M. Alsaari, X.-J. She, L. Liang, J. Zhang, S. Lilliu, P. Gao, H. J. Snaith, J. Wang, N. C. Greenham, R. H. Friend, D. Di, High-efficiency perovskite-polymer bulk heterostructure light-emitting diodes. *Nat. Photonics* **12**, 783–789 (2018).
22. Y. Liu, J. Cui, K. Du, H. Tian, Z. He, Q. Zhou, Z. Yang, Y. Deng, D. Chen, X. Zuo, Y. Ren, L. Wang, H. Zhu, B. Zhao, D. Di, J. Wang, R. H. Friend, Y. Jin, Efficient blue light-emitting diodes based on quantum-confined bromide perovskite nanostructures. *Nat. Photonics* **13**, 760–764 (2019).
23. W. Xu, Q. Hu, S. Bai, C. Bao, Y. Miao, Z. Yuan, T. Borzda, A. J. Barker, E. Tyukalova, Z. Hu, M. Kaweckı, H. Wang, Z. Yan, X. Liu, X. Shi, K. Uvdal, M. Fahlman, W. Zhang, M. Duchamp, J.-M. Liu, A. Petrozza, J. Wang, L.-M. Liu, W. Huang, F. Gao, Rational molecular passivation for high-performance perovskite light-emitting diodes. *Nat. Photonics* **13**, 418–424 (2019).
24. B. Zhao, Y. Lian, L. Cui, G. Divitini, G. Kusch, E. Ruggeri, F. Auras, W. Li, D. Yang, B. Zhu, R. A. Oliver, J. L. MacManus-Driscoll, S. D. Stranks, D. Di, R. H. Friend, Efficient light-emitting diodes from mixed-dimensional perovskites on a fluoride interface. *Nat. Electron.* **3**, 704–710 (2020).
25. Y. Dong, Y. K. Wang, F. Yuan, A. Johnston, Y. Liu, D. Ma, M. J. Choi, B. Chen, M. Chekini, S. W. Baek, L. K. Sagar, J. Fan, Y. Hou, M. Wu, S. Lee, B. Sun, S. Hoogland, R. Quintero-Bermudez, H. Ebe, P. Todorovic, F. Dinic, P. Li, H. T. Kung, M. I. Saidaminov, E. Kumacheva, E. Spiecker, L. S. Liao, O. Voznyy, Z. H. Lu, E. H. Sargent, Bipolar-shell resurfacing for blue LEDs based on strongly confined perovskite quantum dots. *Nat. Nanotechnol.* **15**, 668–674 (2020).
26. Y.-H. Kim, S. Kim, A. Kakekhani, J. Park, J. Park, Y.-H. Lee, H. Xu, S. Nagane, R. B. Wexler, D.-H. Kim, S. H. Jo, L. Martínez-Sarti, P. Tan, A. Sadhanala, G.-S. Park, Y.-W. Kim, B. Hu, H. J. Bolink, S. Yoo, R. H. Friend, A. M. Rappe, T.-W. Lee, Comprehensive defect suppression in perovskite nanocrystals for high-efficiency light-emitting diodes. *Nat. Photonics* **15**, 148–155 (2021).
27. Y. Q. Zhao, Q. R. Ma, B. Liu, Z. L. Yu, M. Q. Cai, Pressure-induced strong ferroelectric polarization in tetra-phase perovskite CsPbBr₃. *Phys. Chem. Phys.* **20**, 14718–14724 (2018).
28. J. Si, Y. Liu, Z. He, H. Du, K. Du, C. Chen, J. Li, M. Xu, H. Tian, H. He, D. Di, C. Lin, Y. Cheng, J. Wang, Y. Jin, Efficient and high-color-purity light-emitting diodes based on in situ grown films of CsPbX₃ (X = Br, I) nanoplates with controlled thicknesses. *ACS Nano* **11**, 11100–11107 (2017).
29. L. Protesescu, S. Yakunin, M. I. Bodnarchuk, F. Kriegel, R. Caputo, C. H. Hendon, R. X. Yang, A. Walsh, M. V. Kovalenko, Nanocrystals of cesium lead halide perovskites (CsPbX₃, X = Cl, Br, and I): Novel optoelectronic materials showing bright emission with wide color gamut. *Nano Lett.* **15**, 3692–3696 (2015).
30. M. A. Becker, R. Vaxenburg, G. Nedelcu, P. C. Sercel, A. Shabaev, M. J. Mehl, J. G. Michopoulos, S. G. Lambrakos, N. Bernstein, J. L. Lyons, T. Stoferle, R. F. Mahrt, M. V. Kovalenko, D. J. Norris, G. Raino, A. L. Efros, Bright triplet excitons in caesium lead halide perovskites. *Nature* **553**, 189–193 (2018).
31. J. Frischeisen, D. Yokoyama, C. Adachi, W. Brutting, Determination of molecular dipole orientation in doped fluorescent organic thin films by photoluminescence measurements. *Appl. Phys. Lett.* **96**, 073302 (2010).
32. H. Shin, J. H. Lee, C. K. Moon, J. S. Huh, B. Sim, J. J. Kim, Sky-blue phosphorescent OLEDs with 34.1% external quantum efficiency using a low refractive index electron transporting layer. *Adv. Mater.* **28**, 4920–4925 (2016).
33. K. A. Neyts, Simulation of light emission from thin-film microcavities. *J. Opt. Soc. Am. A* **15**, 962–971 (1998).
34. W. Lukosz, R. E. Kunz, Light emission by magnetic and electric dipoles close to a plane interface. I. Total radiated power. *J. Opt. Soc. Am.* **67**, 1607–1615 (1977).
35. J. A. Schuller, S. Karaveli, T. Schiros, K. He, S. Yang, I. Kymissis, J. Shan, R. Zia, Orientation of luminescent excitons in layered nanomaterials. *Nat. Nanotechnol.* **8**, 271–276 (2013).
36. A. Rodina, A. L. Efros, Effect of dielectric confinement on optical properties of colloidal nanostructures. *J. Exp. Theor. Phys.* **122**, 554–566 (2016).
37. A. Z. Chen, M. Shiu, J. H. Ma, M. R. Alpert, D. Zhang, B. J. Foley, D.-M. Smilgies, S.-H. Lee, J. J. Choi, Origin of vertical orientation in two-dimensional metal halide perovskites and its effect on photovoltaic performance. *Nat. Commun.* **9**, 1338 (2018).
38. S.-T. Ha, R. Su, J. Xing, Q. Zhang, Q. Xiong, Metal halide perovskite nanomaterials: Synthesis and applications. *Chem. Sci.* **8**, 2522–2536 (2017).
39. R. Quintero-Bermudez, A. Gold-Parker, A. H. Proppe, R. Munir, Z. Yang, S. O. Kelley, A. Amassian, M. F. Toney, E. H. Sargent, Compositional and orientational control in metal halide perovskites of reduced dimensionality. *Nat. Mater.* **17**, 900–907 (2018).
40. H. Wang, X. Zhang, Q. Wu, F. Cao, D. Yang, Y. Shang, Z. Ning, W. Zhang, W. Zheng, Y. Yan, S. V. Kershaw, L. Zhang, A. L. Rogach, X. Yang, Trifluoroacetate induced small-grained CsPbBr₃ perovskite films result in efficient and stable light-emitting devices. *Nat. Commun.* **10**, 665 (2019).
41. Y. Shen, L. P. Cheng, Y. Q. Li, W. Li, J. D. Chen, S. T. Lee, J. X. Tang, High-efficiency perovskite light-emitting diodes with synergetic outcoupling enhancement. *Adv. Mater.* **31**, 1901517 (2019).
42. T. Chiba, Y. Hayashi, H. Ebe, K. Hoshi, J. Sato, S. Sato, Y.-J. Pu, S. Ohisa, J. Kido, Anion-exchange red perovskite quantum dots with ammonium iodine salts for highly efficient light-emitting devices. *Nat. Photonics* **12**, 681–687 (2018).
43. S. Nam, N. Oh, Y. Zhai, M. Shim, High efficiency and optical anisotropy in double-heterojunction nanorod light-emitting diodes. *ACS Nano* **9**, 878–885 (2015).
44. S. Kumar, J. Jagielski, S. Yakunin, P. Rice, Y. C. Chiu, M. Wang, G. Nedelcu, Y. Kim, S. Lin, E. J. Santos, M. V. Kovalenko, C. J. Shih, Efficient blue electroluminescence using quantum-confined two-dimensional perovskites. *ACS Nano* **10**, 9720–9729 (2016).
45. W. D. Kim, D. Kim, D.-E. Yoon, H. Lee, J. Lim, W. K. Bae, D. C. Lee, Pushing the efficiency envelope for semiconductor nanocrystal-based electroluminescence devices using anisotropic nanocrystals. *Chem. Mater.* **31**, 3066–3082 (2019).
46. Y. Ling, Z. Yuan, Y. Tian, X. Wang, J. C. Wang, Y. Xin, K. Hanson, B. Ma, H. Gao, Bright light-emitting diodes based on organometal halide perovskite nanoplatelets. *Adv. Mater.* **28**, 305–311 (2016).
47. F. Li, L. Yang, Z. Cai, K. Wei, F. Lin, J. You, T. Jiang, Y. Wang, X. Chen, Enhancing exciton binding energy and photoluminescence of formamidinium lead bromide by reducing its dimensions to 2D nanoplates for producing efficient light emitting diodes. *Nanoscale* **10**, 20611–20617 (2018).
48. J. R. Manders, S.-W. Tsang, M. J. Hartel, T.-H. Lai, S. Chen, C. M. Amb, J. R. Reynolds, F. So, Solution-processed nickel oxide hole transport layers in high efficiency polymer photovoltaic cells. *Adv. Funct. Mater.* **23**, 2993–3001 (2013).
49. X. Dai, Z. Zhang, Y. Jin, Y. Niu, H. Cao, X. Liang, L. Chen, J. Wang, X. Peng, Solution-processed, high-performance light-emitting diodes based on quantum dots. *Nature* **515**, 96–99 (2014).
50. J. Song, T. Fang, J. Li, L. Xu, F. Zhang, B. Han, Q. Shan, H. Zeng, Organic-inorganic hybrid passivation enables perovskite QLEDs with an EQE of 16.48%. *Adv. Mater.* **30**, 1805409 (2018).
51. S. Kumar, J. Jagielski, C.-J. Shih, Quantum confined colloidal perovskite nanoplatelets for extremely pure green and efficient LEDs, in *Novel Optical Materials and Applications* (Optical Society of America, 2018), pp. NoTu3C.2.
52. X. Hu, H. Zhou, Z. Jiang, X. Wang, S. Yuan, J. Lan, Y. Fu, X. Zhang, W. Zheng, X. Wang, X. Zhu, L. Liao, G. Xu, S. Jin, A. Pan, Direct vapor growth of perovskite CsPbBr₃ nanoplate electroluminescence devices. *ACS Nano* **11**, 9869–9876 (2017).

53. R. L. Hoye, M.-L. Lai, M. Anaya, Y. Tong, K. Gałkowski, T. Doherty, W. Li, T. N. Huq, S. Mackowski, L. Polavarapu, J. Feldmann, J. L. Mac Manus-Driscoll, R. H. Friend, A. S. Urban, S. D. Stranks, Identifying and reducing interfacial losses to enhance color-pure electroluminescence in blue-emitting perovskite nanoplatelet light-emitting diodes. *ACS Energy Lett.* **4**, 1181–1188 (2019).
54. S. Kumar, J. Jagielski, N. Kallikounis, Y. H. Kim, C. Wolf, F. Jenny, T. Tian, C. J. Hofer, Y. C. Chiu, W. J. Stark, T. W. Lee, C. J. Shih, Ultrapure green light-emitting diodes using two-dimensional formamidinium perovskites: Achieving recommendation 2020 color coordinates. *Nano Lett.* **17**, 5277–5284 (2017).
55. D. Yang, Y. Zou, P. Li, Q. Liu, L. Wu, H. Hu, Y. Xu, B. Sun, Q. Zhang, S.-T. Lee, Large-scale synthesis of ultrathin cesium lead bromide perovskite nanoplates with precisely tunable dimensions and their application in blue light-emitting diodes. *Nano Energy* **47**, 235–242 (2018).
56. A. B. Wong, M. Lai, S. W. Eaton, Y. Yu, E. Lin, L. Dou, A. Fu, P. Yang, Growth and anion exchange conversion of $\text{CH}_3\text{NH}_3\text{PbX}_3$ nanorod arrays for light-emitting diodes. *Nano Lett.* **15**, 5519–5524 (2015).
57. B. Liu, S. Delikanli, Y. Gao, D. Dede, K. Gungor, H. V. Demir, Nanocrystal light-emitting diodes based on type II nanoplatelets. *Nano Energy* **47**, 115–122 (2018).
58. Z. Chen, B. Nadal, B. Mahler, H. Aubin, B. Dubertret, Quasi-2D colloidal semiconductor nanoplatelets for narrow electroluminescence. *Adv. Funct. Mater.* **24**, 295–302 (2014).
59. U. Giovanella, M. Pasini, M. Lorenzon, F. Galeotti, C. Lucchi, F. Meinardi, S. Luzzati, B. Dubertret, S. Brovelli, Efficient solution-processed nanoplatelet-based light-emitting diodes with high operational stability in air. *Nano Lett.* **18**, 3441–3448 (2018).
60. F. Zhang, S. Wang, L. Wang, Q. Lin, H. Shen, W. Cao, C. Yang, H. Wang, L. Yu, Z. Du, J. Xue, L. S. Li, Super color purity green quantum dot light-emitting diodes fabricated by using CdSe/CdS nanoplatelets. *Nanoscale* **8**, 12182–12188 (2016).
61. R. A. M. Hikmet, P. T. K. Chin, D. V. Talapin, H. Weller, Polarized-light-emitting quantum-rod diodes. *Adv. Mater.* **17**, 1436–1439 (2005).
62. N. Oh, S. Nam, Y. Zhai, K. Deshpande, P. Trefonas, M. Shim, Double-heterojunction nanorods. *Nat. Commun.* **5**, 3642 (2014).
63. P. Rastogi, F. Palazon, M. Prato, F. Di Stasio, R. Krahn, Enhancing the performance of CdSe/CdS dot-in-rod light-emitting diodes via surface ligand modification. *ACS Appl. Mater. Inter.* **10**, 5665–5672 (2018).
64. A. Castelli, F. Meinardi, M. Pasini, F. Galeotti, V. Pinchetti, M. Lorenzon, L. Manna, I. Moreels, U. Giovanella, S. Brovelli, High-efficiency all-solution-processed light-emitting diodes based on anisotropic colloidal heterostructures with polar polymer injecting layers. *Nano Lett.* **15**, 5455–5464 (2015).
65. Y. Jiang, N. Oh, M. Shim, Double-heterojunction nanorod light-emitting diodes with high efficiencies at high brightness using self-assembled monolayers. *ACS Photonics* **3**, 1862–1868 (2016).

Acknowledgments: We thank X. Zeng and C. Yang (Wuhan University, China) for assistance with the angle-dependent PL measurements. We thank W. Fang (Zhejiang University, China) for the inspiring discussions on the characterizations of the optical properties of the perovskite films. This research used resources of the Advanced Photon Source, a U.S. Department of Energy (DOE) Office of Science User Facility operated for the DOE Office of Science by Argonne National Laboratory under contract no. DE-AC02-06CH11357. **Funding:** This work was financially supported by the National Key R&D Program of China (2016YFB0401600), the National Natural Science Foundation of China (91833303, 51911530155, 91733302, and 62005243), the Fundamental Research Funds for the Central Universities (2017XZZX001-03A and 2020QNA5002), the Key Research and Development Program of Zhejiang Province (2021C01030), the Natural Science Foundation of Zhejiang Province (LR21F050003), and China National Postdoctoral Program for Innovative Talents (BX20200288). **Author contributions:** Y.J. and Y.L. conceived the idea and designed the experiments. Y.J. and Z.Y. supervised the work. J.C. carried out the device fabrication. J.C. and Y.L. carried out the device characterizations. Y.D. carried out the optical simulation of our perovskite devices. J.C., Y.L., C.L., and Z.F. conducted the optical measurements. P.B. and Y.G. did the BFP measurement. J.C. synthesized the PBABr and NiO_x . C.X., K.D., and H.T. carried out the STEM and HRTEM characterizations. X.Z. conducted the GIWAXS measurements. C.L. and Y.D. carried out the AFM experiments. B.Z. cross-checked the LED measurements. K.W. conducted the measurements of the angular dependence of EL emission. Y.J., J.C., and Y.L. wrote the first draft of the manuscript. H.H., Z.Y., Y.G., and J.W. participated in data analysis. All authors discussed the results and commented on the manuscript. **Competing interests:** The authors declare that they have no competing interests. **Data and materials availability:** All data needed to evaluate the conclusions in the paper are present in the paper and/or the Supplementary Materials.

Submitted 31 January 2021

Accepted 19 August 2021

Published 8 October 2021

10.1126/sciadv.abg8458

Citation: J. Cui, Y. Liu, Y. Deng, C. Lin, Z. Fang, C. Xiang, P. Bai, K. Du, X. Zuo, K. Wen, S. Gong, H. He, Z. Ye, Y. Gao, H. Tian, B. Zhao, J. Wang, Y. Jin, Efficient light-emitting diodes based on oriented perovskite nanoplatelets. *Sci. Adv.* **7**, eabg8458 (2021).